doi:10.1093/brain/aws327 Brain 2013: 136; 844–858 | 844

BRAIN
A JOURNAL OF NEUROLOGY

Diverging patterns of amyloid deposition and hypometabolism in clinical variants of probable Alzheimer's disease

Manja Lehmann,[1,2,3] Pia M. Ghosh,[1,2] Cindee Madison,[2] Robert Laforce Jr,[1,2] Chiara Corbetta-Rastelli,[2] Michael W. Weiner,[4] Michael D. Greicius,[5] William W. Seeley,[1] Maria L. Gorno-Tempini,[1] Howard J. Rosen,[1] Bruce L. Miller,[1] William J. Jagust[1,2,6] and Gil D. Rabinovici[1,2,6]

1 Memory and Ageing Centre, Department of Neurology, University of California, San Francisco, CA 94158, USA
2 Helen Wills Neuroscience Institute, University of California, Berkeley, CA 94720, USA
3 Dementia Research Centre, Institute of Neurology, University College London, Queen Square, London, WC1N 3BG, UK
4 Centre for Imaging of Neurodegenerative Diseases, Department of Veterans Affairs Medical Centre, San Francisco, CA 94121, USA
5 Functional Imaging in Neuropsychiatric Disorders (FIND) Laboratory, Department of Neurology and Neurological Sciences, Stanford University School of Medicine, Stanford, CA 94305, US
6 Lawrence Berkeley National Laboratory, Department of Radiology, University of California, Berkeley, CA 94720, USA

Correspondence to: Manja Lehmann,
UCSF Memory and Ageing Centre,
Department of Neurology,
Box 1207, San Francisco,
CA 94158-1207
E-mail: mlehmann@memory.ucsf.edu

The factors driving clinical heterogeneity in Alzheimer's disease are not well understood. This study assessed the relationship between amyloid deposition, glucose metabolism and clinical phenotype in Alzheimer's disease, and investigated how these relate to the involvement of functional networks. The study included 17 patients with early-onset Alzheimer's disease (age at onset <65 years), 12 patients with logopenic variant primary progressive aphasia and 13 patients with posterior cortical atrophy [whole Alzheimer's disease group: age = 61.5 years (standard deviation 6.5 years), 55% male]. Thirty healthy control subjects [age = 70.8 (3.3) years, 47% male] were also included. Subjects underwent positron emission tomography with ^{11}C-labelled Pittsburgh compound B and ^{18}F-labelled fluorodeoxyglucose. All patients met National Institute on Ageing–Alzheimer's Association criteria for probable Alzheimer's disease and showed evidence of amyloid deposition on ^{11}C-labelled Pittsburgh compound B positron emission tomography. We hypothesized that hypometabolism patterns would differ across variants, reflecting involvement of specific functional networks, whereas amyloid patterns would be diffuse and similar across variants. We tested these hypotheses using three complimentary approaches: (i) mass-univariate voxel-wise group comparison of ^{18}F-labelled fluorodeoxyglucose and ^{11}C-labelled Pittsburgh compound B; (ii) generation of covariance maps across all subjects with Alzheimer's disease from seed regions of interest specifically atrophied in each variant, and comparison of these maps to functional network templates; and (iii) extraction of ^{11}C-labelled Pittsburgh compound B and ^{18}F-labelled fluorodeoxyglucose values from functional network templates. Alzheimer's disease clinical groups showed syndrome-specific ^{18}F-labelled fluorodeoxyglucose patterns, with greater parieto-occipital involvement in posterior cortical atrophy, and asymmetric involvement of left temporoparietal regions in logopenic variant primary progressive aphasia. In contrast, all Alzheimer's disease variants showed diffuse patterns of ^{11}C-labelled Pittsburgh compound B binding, with posterior cortical atrophy additionally showing elevated uptake in occipital cortex compared with early-onset Alzheimer's disease. The seed region of interest covariance

Received June 12, 2012. Revised September 24, 2012. Accepted October 17, 2012. Advance Access publication January 28, 2013

analysis revealed distinct ^{18}F-labelled fluorodeoxyglucose correlation patterns that greatly overlapped with the right executive-control network for the early-onset Alzheimer's disease region of interest, the left language network for the logopenic variant primary progressive aphasia region of interest, and the higher visual network for the posterior cortical atrophy region of interest. In contrast, ^{11}C-labelled Pittsburgh compound B covariance maps for each region of interest were diffuse. Finally, ^{18}F-labelled fluorodeoxyglucose was similarly reduced in all Alzheimer's disease variants in the dorsal and left ventral default mode network, whereas significant differences were found in the right ventral default mode, right executive-control (both lower in early-onset Alzheimer's disease and posterior cortical atrophy than logopenic variant primary progressive aphasia) and higher-order visual network (lower in posterior cortical atrophy than in early-onset Alzheimer's disease and logopenic variant primary progressive aphasia), with a trend towards lower ^{18}F-labelled fluorodeoxyglucose also found in the left language network in logopenic variant primary progressive aphasia. There were no differences in ^{11}C-labelled Pittsburgh compound B binding between syndromes in any of the networks. Our data suggest that Alzheimer's disease syndromes are associated with degeneration of specific functional networks, and that fibrillar amyloid-β deposition explains at most a small amount of the clinico-anatomic heterogeneity in Alzheimer's disease.

Keywords: Alzheimer's disease; posterior cortical atrophy; logopenic variant of PPA; positron emission tomography (PET); functional networks

Abbreviations: FDG = fluorodeoxyglucose; MMSE = Mini-Mental State Examination; PIB = Pittsburgh compound B; PPA = primary progressive aphasia

Introduction

Although episodic memory loss is considered the clinical hallmark of Alzheimer's disease, a significant number of patients with underlying Alzheimer's disease pathology present with focal, non-amnestic clinical syndromes. Patients with early age-of-onset Alzheimer's disease (defined as <65 years in most studies) tend to show more heterogeneous neuropsychological deficits, including greater impairment in attention, executive, visuospatial and language functions, and relatively spared memory compared with patients with late age-of-onset (Koss *et al.*, 1996; Frisoni *et al.*, 2007; Koedam *et al.*, 2010). Alzheimer's disease pathology is also the most common cause of two focal cortical syndromes associated with early age-of-onset: posterior cortical atrophy, a condition characterized by predominant visuospatial and visuoperceptual dysfunction (Benson *et al.*, 1988; Crutch *et al.*, 2012), and the logopenic variant of primary progressive aphasia (PPA), a progressive disorder of language (Gorno-Tempini *et al.*, 2008; Mesulam *et al.*, 2008). It has been suggested that up to 15% of patients with Alzheimer's disease seen in dementia centres have non-amnestic presentations (Snowden *et al.*, 2007), and the importance of these syndromes is reflected in their inclusion in new diagnostic guidelines for Alzheimer's disease (McKhann *et al.*, 2011). A better understanding of the factors that drive the heterogeneity of these clinical phenotypes may yield important insights into Alzheimer's disease mechanisms and have direct implications for diagnosis and management of non-amnestic patients with emerging disease-specific therapies.

The pattern of neurodegeneration in Alzheimer's disease variants is highly correlated with the clinical syndrome. Compared with 'typical' amnestic late-onset Alzheimer's disease, patients with early-onset Alzheimer's disease show relative sparing of the medial temporal lobes and greater atrophy in temporoparietal and lateral prefrontal cortex (Frisoni *et al.*, 2005; Shiino *et al.*, 2008; Rabinovici *et al.*, 2010). Patients with posterior cortical atrophy and logopenic variant PPA show strikingly focal patterns of neurodegeneration, with greater bilateral occipito-parietal atrophy and hypometabolism in posterior cortical atrophy and highly asymmetric left temporoparietal involvement in logopenic variant PPA (Whitwell *et al.*, 2007; Rabinovici *et al.*, 2008; Migliaccio *et al.*, 2009; Rosenbloom *et al.*, 2010; Lehmann *et al.*, 2011).

There have been conflicting reports in the literature regarding the relationship between the distribution of Alzheimer's disease pathology and the region-specific neurodegenerative patterns seen in Alzheimer's disease variants. Some autopsy studies have reported an increased burden of both amyloid plaques and neurofibrillary tangles in visual regions in posterior cortical atrophy (Levine *et al.*, 1993; Ross *et al.*, 1996; Hof *et al.*, 1997), whereas others have found increases in tangle, but not plaque burden (Renner *et al.*, 2004; Tang-Wai *et al.*, 2004). Similarly, pathology studies in PPA due to Alzheimer's disease have more frequently found an increased burden of tangles than plaques in the left hemisphere compared with amnestic Alzheimer's disease (Mesulam *et al.*, 2008; Gefen *et al.*, 2012), though this is highly variable across patients and between studies (Galton *et al.*, 2000; Knibb *et al.*, 2006). *In vivo* studies using PET with the amyloid-β-specific tracer Pittsburgh compound B (PIB) have reported greater PIB uptake in occipital cortex in posterior cortical atrophy (Ng *et al.*, 2007; Tenovuo *et al.*, 2008; Kambe *et al.*, 2010; Formaglio *et al.*, 2011), and left temporoparietal regions in PPA (Ng *et al.*, 2007) in single cases and small series studies, whereas larger group studies have found no differences in PIB retention patterns in posterior cortical atrophy or PPA versus amnestic Alzheimer's disease (Rabinovici *et al.*, 2008; Rosenbloom *et al.*, 2010; de Souza *et al.*, 2011; Leyton *et al.*, 2011). To our knowledge, no study has compared patterns of amyloid aggregation and neurodegeneration across three common clinical phenotypes of early age-of-onset Alzheimer's disease. A better characterization of the relationship between clinico-anatomical heterogeneity in Alzheimer's disease and

amyloid is particularly timely, given the emergence of therapies that specifically target amyloid-β pathology (Holmes *et al.*, 2008; Salloway *et al.*, 2009).

Converging data from animal models and human imaging studies support the hypothesis that Alzheimer's disease spreads through interconnected neural networks (Clavaguera *et al.*, 2009; de Calignon *et al.*, 2012; Zhou *et al.*, 2012). In transgenic mice, neurofibrillary pathology appears to spread sequentially from synapse to synapse, ultimately reflecting the pattern of structural connectivity (Clavaguera *et al.*, 2009; de Calignon *et al.*, 2012). Neuroimaging studies in humans demonstrate that disease-specific atrophy patterns closely match functional connectivity maps in cognitively normal individuals, suggesting that Alzheimer's disease and other neurodegenerative disorders target specific functional networks (Seeley *et al.*, 2009; Zhou *et al.*, 2012). In Alzheimer's disease, many studies have demonstrated disruption of the default mode network in typical amnestic patients (Greicius *et al.*, 2004; Wang *et al.*, 2007), including in the pre-dementia phase (Rombouts *et al.*, 2005; Sorg *et al.*, 2007; Sheline *et al.*, 2010; Mormino *et al.*, 2011). This finding is particularly compelling considering that disruptions to the default mode network are associated with poor performance on memory tests (Otten and Rugg, 2001; Grady *et al.*, 2006; Miller *et al.*, 2008; Sambataro *et al.*, 2010). It is therefore conceivable that the disproportionate visual and language deficits seen in patients with posterior cortical atrophy and logopenic variant PPA may reflect spread of disease through visual and language networks, respectively, whereas the high incidence of executive and attention difficulties in patients with early-onset Alzheimer's disease may indicate involvement of the executive-control network. This model would suggest that Alzheimer's disease pathology may originate in a common network, most likely the default mode network, and that clinical heterogeneity in Alzheimer's disease reflects differential dissemination of pathology from the default mode network into distinct 'off-target' functional networks.

In this study, we sought to compare patterns of amyloid deposition (PIB-PET) and neurodegeneration [fluorodeoxyglucose (FDG)-PET)] across three primary clinical phenotypes of early age-of-onset Alzheimer's disease. These less common Alzheimer's disease variants were chosen over the more common late-onset amnestic variant of Alzheimer's disease to maximize heterogeneity in our study population and increase the likelihood of identifying the mechanisms that contribute to the clinico-anatomic variance of the disease. Our hypothesis was that neurodegeneration in the three Alzheimer's disease variants follows distinct patterns that mirror the involvement of specific functional networks: executive-control in early-onset Alzheimer's disease, language in logopenic variant PPA and higher-order visual in posterior cortical atrophy, whereas the default mode network is a core network that is involved in all three variants. We further predicted that distinct patterns of neurodegeneration in the three Alzheimer's disease variants would not be explained by patterns of amyloid deposition. We tested these hypotheses using three complimentary approaches: (i) traditional mass-univariate voxel-wise group comparisons; (ii) generation of covariance maps across all subjects with Alzheimer's disease from seed regions of interest shown to be specifically affected in each variant, and comparison of these maps with functional network templates; and (iii) extraction of PIB and ^{18}F-labelled FDG values from templates of well-described functional networks.

Materials and methods

Subjects

Patients with early-onset Alzheimer's disease, logopenic variant PPA and posterior cortical atrophy were recruited from research cohorts at the University of California San Francisco (UCSF) Memory and Ageing Centre. All patients underwent a history and physical examination by a neurologist, a structured caregiver interview by a nurse and a battery of neuropsychological tests (Kramer *et al.*, 2003). Clinical diagnosis was assigned by consensus at a multidisciplinary conference. Clinicians were blinded to PET results at the time of diagnosis.

All patients had at least one usable FDG-PET, PIB-PET and MRI scan. All subjects fulfilled criteria for probable Alzheimer's disease according to the National Institute on Ageing–Alzheimer's Association criteria (McKhann *et al.*, 2011) and showed evidence of amyloid deposition on PIB-PET. Patients were excluded if they presented with core features of other dementias, such as dementia with Lewy bodies, therefore reducing the likelihood of underlying co-pathologies that are associated with amyloid-β deposition. Patients with posterior cortical atrophy and logopenic variant PPA were initially selected based on their clinical diagnosis. Clinical and neuropsychological reports were then reviewed to assess whether patients fulfilled specific diagnostic criteria (logopenic variant PPA: Gorno-Tempini *et al.*, 2011; posterior cortical atrophy: Mendez *et al.*, 2002; Tang-Wai *et al.*, 2004). Patients with early-onset Alzheimer's disease had an age of onset <65 years and did not meet criteria for posterior cortical atrophy and logopenic variant PPA. Early age-of-onset patients were chosen over late-onset patients to allow us to match this group to the relatively young logopenic variant PPA and posterior cortical atrophy groups. The selection of clinical phenotypes in this study also matched the clinical variants included in Migliaccio *et al*. (2009) from which seed regions of interest for the covariance analysis were identified (see later in the text).

The final cohort consisted of 17 patients with early-onset Alzheimer's disease, 12 patients with logopenic variant PPA and 13 patients with posterior cortical atrophy. Demographics and clinical data are summarized in Table 1. A proportion of these patients were included in previous PET studies [31% of patients with posterior cortical atrophy and 59% of patients with early-onset Alzheimer's disease in Rabinovici *et al.* (2010); three patients with logopenic variant PPA (25%) in Rabinovici *et al.* (2008); 77% of patients with posterior cortical atrophy and 35% of patients with early-onset Alzheimer's disease in Rosenbloom *et al.* (2010)]. Thirty healthy control subjects were included for comparison. The majority of the control subjects (27 of the 30) were recruited as part of the Berkeley Ageing Cohort (Mormino *et al.*, 2009), with three subjects recruited at the UCSF. Selection of control participants was primarily based on the availability of PET scans. Of those control subjects with PET scans, we selected the youngest 30 participants to match the mean age of the control group to that of the patient group. The Berkeley Ageing Cohort eligibility criteria include a minimum age of 60 years, which prevented more accurate age-matching of control subjects to patients. Further eligibility criteria included normal performance on cognitive tests, absence of neurological or psychiatric illness and lack of major medical illnesses and medications that affect cognition (Mormino *et al.*, 2009).

Table 1 Subject demographics

	Control subjects	EOAD	lvPPA	PCA	P[a]
n	30	17	12	13	
Sex % male	47	59	67	46	0.8[b]
Age, years[c]	70.8 (3.3)	60.7 (5.6)	61.4 (7.0)	62.6 (7.4)	<0.0001
Education, years	17.6 (1.7)	16.9 (2.7)	16.6 (3.1)	15.8 (3.0)	0.2
MMSE (/30)	29.4 (0.9)	19.9 (7.2)	22.4 (6.7)	21.7 (5.6)	<0.0001
ApoE ε4 % carrier[d]	33	63	25	36	0.2[b]
Age at onset, years		56.3 (5.6)	56.9 (6.7)	57.8 (7.1)	0.8
Disease duration, years[e]		4.5 (2.5)	4.5 (2.0)	4.8 (2.8)	0.9

Shown are mean (standard deviation) unless specified otherwise.
a one-way analysis of variance across groups (except sex and ApoE ε4).
b Fisher's exact test.
c Age at time of PET scan.
d ApoE available in 30 control subjects and 39 patients with Alzheimer's disease (16 with early-onset Alzheimer's disease, 12 with logopenic variant PPA and11 with posterior cortical atrophy).
e Time between first symptoms and PET scan.
EOAD = early-onset Alzheimer's disease; lvPPA = logopenic variant PPA; PCA = posterior cortical atrophy.

Informed consent was obtained from all subjects or their assigned surrogate decision-makers, and the study was approved by the University of California Berkeley, the UCSF and the Lawrence Berkeley National Laboratory institutional review boards for human research.

Positron emission tomography image acquisition and preprocessing

All subjects underwent PET imaging with ^{11}C-PIB and ^{18}F-FDG at Lawrence Berkeley National Laboratory on a Siemens ECAT EXACT HR PET scanner in 3D acquisition mode. Tracer synthesis, PET acquisition and preprocessing are described in detail in the online Supplementary material. For PIB, voxel-wise distribution volume ratios were calculated using Logan graphical analysis (Logan *et al.*, 1996) with the grey matter cerebellum time–activity curve used as a reference tissue input function (Price *et al.*, 2005). FDG-PET frames were summed and standard uptake volume ratios were calculated by normalizing the summed FDG image to mean activity in the pons for each subject (Minoshima *et al.*, 1995). PIB and FDG volumes were spatially normalized to Montreal Neurological Institute (MNI) space. All normalized images were smoothed with a 12-mm kernel. In a *post hoc* analysis, we corrected PET data for atrophy by applying a two-compartmental partial volume correction (Meltzer *et al.*, 1990) (Supplementary material).

Magnetic resonance image acquisition and processing

T_1-weighted scans were collected on different MRI units, including two 1.5 T units (Magnetom Avanto System, Siemens Medical Systems; Magneton VISION system, Siemens Inc), one 3 T unit (Siemens Tim Trio scanner) and one 4 T unit (BrukerMedSpec). Acquisition parameters for all scanners have been previously described (Rosen *et al.*, 2002; Mueller *et al.*, 2009; Mormino *et al.*, 2012; Zhou *et al.*, 2012). The proportions of subjects studied on each scanner were balanced across the three Alzheimer's disease groups, although 90% of control subjects were studied on a single 1.5 T scanner. Anatomical scans were processed using FreeSurfer version 4.5 (http://surfer.nmr.mgh.harvard.edu; Dale *et al.*, 1999) to generate subcortical parcellations used for defining subject-specific reference regions.

Positron emission tomography image analysis

PET data were analysed using three different approaches: (i) mass-univariate voxel-wise group comparisons of FDG and PIB; (ii) generation of covariance maps across all subjects with Alzheimer's disease from seed regions of interest shown to be specifically atrophied in each Alzheimer's disease variant and comparison of these maps to functional network templates; and (iii) extraction of PIB and FDG values from functional network templates. Although different, these three approaches provide complimentary data that, together, strengthen our findings and interpretations about the relationship between amyloid, hypometabolism, functional networks and clinical Alzheimer's disease phenotype.

Voxel-wise group comparisons

Voxel-wise comparisons of PIB distribution volume ratio and FDG standard uptake volume ratio images were performed in SPM8 using an analysis of covariance model that included diagnosis (control subjects, early-onset Alzheimer's disease, logopenic variant PPA and posterior cortical atrophy) as the condition, and age, sex and education as covariates. Pairwise contrasts were performed among the four groups. This analysis was repeated including Mini-Mental State Examination (MMSE) scores (Folstein *et al.*, 1975) as covariate to adjust group-wise comparisons for disease severity. All voxel-wise comparisons were also repeated with atrophy-corrected data. Resulting T-maps were displayed on an MNI template brain corrected for multiple comparisons using a family-wise error (FWE) correction at $P < 0.05$.

Voxel-wise region of interest correlation analysis

We extracted PIB and FDG values from regions of interest previously shown to be specifically affected in each Alzheimer's disease variant compared with the other two and applied these values as covariates in a voxel-wise multi-linear regression model to identify regions that

showed correlated PIB or FDG uptake across the brain in all patients with Alzheimer's disease. This approach is analogous to the seed correlation method used to identify networks of structural and functional connectivity (Seeley *et al.*, 2009) and was used to explore whether we could identify region of interest-specific patterns of PIB and FDG uptake that were not detected using traditional voxel-wise comparisons of clinically defined groups.

Region of interest definitions

The seed regions of interest used in this analysis were based on peak atrophy voxels defined in a previous study (Migliaccio *et al.*, 2009) that used voxel-based morphometry in early-onset Alzheimer's disease, logopenic variant PPA and posterior cortical atrophy to identify regions that were specifically atrophied in each variant compared with the other two. These were found to be the right middle frontal gyrus in early-onset Alzheimer's disease (MNI 40 42 30), left superior temporal sulcus in logopenic variant PPA (MNI −56 −40 1) and the right middle occipital gyrus in posterior cortical atrophy (MNI 39 −88 10). Regions of interest were created by drawing 6-mm spheres around the peak atrophy voxels (Supplementary Fig. 1). FDG standard uptake volume ratio and PIB distribution volume ratio values were extracted for each region of interest, masking by the individual's grey matter segmented images to exclude PET counts from white matter and cerebrospinal fluid. There was some overlap in the cohorts used in the study by Migliaccio *et al*. (2009) and the current study [six patients with early-onset Alzheimer's disease (four with same scan, two with scans from different time points), three patients with logopenic variant PPA (one with same scan, two with scans from different time points) and three patients with posterior cortical atrophy (one with same scan, two with scans from different time points)]. All analyses were repeated excluding these subjects, producing very similar results (data not shown).

Correlation analysis

Multiple regressions were performed in SPM8 to assess correlations between FDG and PIB uptake in each seed region of interest with FDG and PIB uptake across the brain. Separate models were used for each seed region of interest and each tracer, resulting in three correlation models for FDG and three models for PIB. Analyses were adjusted for age, sex, education and MMSE. Regressions were conducted with all Alzheimer's disease subjects pooled together (i.e. not including the control subjects and not distinguishing between Alzheimer's disease clinical variants). The decision to perform this analysis in the subjects with Alzheimer's disease rather than the control subjects was based on the fact that there is greater variability of FDG values in the Alzheimer's disease group than the control subjects (as control subjects typically have consistently high FDG values), and there is a higher number of PIB-positive subjects available in the Alzheimer's disease group, which increases the power to detect effects. To assess whether results are driven by individual clinical phenotypes, the analysis was repeated adjusting for diagnosis (Supplementary Fig. 2). These analyses were also repeated using atrophy-corrected data. T-maps were produced showing statistically significant correlations using FWE-correction at $P < 0.05$. Overlap maps were produced by overlaying correlation maps for each seed region of interest onto the same MNI template brain.

Goodness of fit

The close resemblance of the correlation maps obtained in the region of interest covariance analysis with specific functional networks motivated a *post hoc* analysis in which we assessed the goodness of fit of the PET correlation maps for each seed region of interest with functional network templates published by the Stanford Functional Imaging in Neuropsychiatric Disorders Lab (Shirer *et al*., 2012). As described in Shirer *et al*. (2012), these networks were created by applying FSL's MELODIC independent component analysis software to resting state data of 15 healthy control subjects. The resulting network templates were downloaded as binary regions of interest from http://findlab.stanford.edu/functional_ROIs.html. A total of 15 network templates are available: dorsal and ventral default mode network, precuneus network, primary and higher visual networks, visuospatial network, language network (which was split into left and right language networks), left and right executive-control networks, anterior and posterior salience networks, sensorimotor network, auditory network and basal ganglia network. Functional connectivity networks have been shown to be reproducible across centres and validated using diffusion tensor imaging tractography and activation functional MRI data (Hampson *et al.*, 2002; Greicius *et al.*, 2009; Smith *et al.*, 2009).

Goodness of fit is expressed as two different variables: (i) as the difference between the mean *z* score of all voxels of the region of interest correlation map (transformed SPM *t*-maps) that fell inside the network template (z_{inside}) and the mean *z*-score of all voxels outside the network template ($z_{outside}$), i.e. goodness of fit = $z_{inside} - z_{outside}$; and (ii) as the ratio between z_{inside} and $z_{outside}$ (i.e. $z_{inside}/z_{outside}$). Furthermore, to assess the robustness of the overlap between the region of interest correlation maps and functional network templates, the goodness of fit analysis was repeated using a second, independent set of network templates, which consisted of networks identified by the 1000 Functional Connectomes Project (http://fcon_1000.projects.nitrc.org; Biswal *et al*., 2010, results shown in the Supplementary material).

Fluorodeoxyglucose and Pittsburgh compound B uptake in functional network templates

FDG standard uptake volume ratio and PIB distribution volume ratio values were extracted from the three network templates that showed the highest fit with the FDG correlation maps (i.e. right executive-control, left language and higher visual network), as well as the dorsal and ventral default mode network based on our hypothesis that the default mode network is affected similarly in all variants. FDG and PIB values in these five networks were compared between groups.

Statistical analysis

Statistical analyses were performed using STATA version 11.2 (STATA Corporation). Group differences in continuous variables were examined using two-tailed independent sample *t*-tests or one-way analysis of variance (ANOVA) and Tukey *post hoc* contrasts. Dichotomous variables were compared with Fisher's exact test.

Results

Subject characteristics

Subject groups were well matched for sex and education (Table 1). Although the control group was older than the patients with Alzheimer's disease ($P < 0.0001$), there was no difference in age between the three Alzheimer's disease clinical groups ($P = 0.7$).

There was no difference in ApoE ε4 status between the four groups; however, there was a trend towards a higher proportion of ApoE ε4 carriers in the group with early-onset Alzheimer's disease compared with logopenic variant PPA ($P = 0.067$). As expected, MMSE scores (obtained closest to PET date) were higher in the control subjects compared with Alzheimer's disease ($P < 0.0001$), but MMSE scores were not different between the three Alzheimer's disease clinical groups ($P = 0.6$). Alzheimer's disease groups showed similar age-at-onset and disease duration.

Neuropsychological profiles

Neuropsychological test batteries obtained within 1 year of PET were available for 16/17 patients with early-onset Alzheimer's disease, 11/12 patients with logopenic variant PPA and 13/13 patients with posterior cortical atrophy (Table 2). The mean interval between cognitive testing and PET was 79.6 days (SD 77.6 days). As expected, patients with early-onset Alzheimer's disease performed poorly on verbal and visual memory tasks, whereas patients with posterior cortical atrophy showed lower performance on visuospatial tasks, as well as face matching and Stroop colour naming. Patients with posterior cortical atrophy also performed worse on the calculation test compared with patients with early-onset Alzheimer's disease ($P = 0.03$ in the direct comparison). The group with logopenic variant PPA performed significantly worse on the digit span forward test, as well as on sentence repetition, both tests that involve phonological loop processing. Naming was also lower in patients with logopenic variant PPA compared with the other two groups; however, this did not reach statistical significance, supporting previous findings that

Table 2 Neuropsychological test scores

Neuropsychological test	EOAD ($n = 16$)	lvPPA ($n = 11$)	PCA ($n = 13$)	*P*-value[a]
MMSE (/30)	21.1 (5.5)	23.0 (6.7)	21.7 (5.6)	0.72
Memory				
CVLT-SF total learning (/36)	14.8 (7.6)	17.0 (7.3)	16.2 (6.9)	0.73
CVLT-SF 10-min recall (/9)	1.1 (2.3)	3.6 (2.5)	2.8 (2.7)	0.04
Modified Rey 10-min recall (/17)	2.8 (3.2)	6.5 (3.0)	2.5 (3.3)	0.01
Language				
Boston Naming Test (/15)	11.9 (3.0)	10.3 (4.2)	11.1 (4.1)	0.54
Syntax comprehension (/5)	3.1 (1.5)	3.3 (1.3)	2.4 (1.7)	0.34
Letter fluency (D words)	9.3 (4.8)	7.3 (3.3)	9.1 (4.1)	0.45
Category fluency (animals)	10.0 (3.6)	8.9 (4.3)	9.8 (4.4)	0.78
Repetition and working memory				
Sentence repetition (/5)	3.1 (1.6)	1.8 (1.0)	3.1 (1.0)	0.03
Digit span forward (/9)	5.0 (1.2)	4.1 (0.7)	5.4 (0.8)	0.04
Digit span backward (/8)	3.2 (1.4)	3.3 (0.8)	2.5 (0.7)	0.17
Executive function				
Modified Trails B time (120s)	94.3 (38.6)	78.7 (34.3)	106.0 (21.3)	0.21
Modified Trails B correct lines/min	10.6 (13.2)	12.5 (9.7)	5.8 (4.7)	0.35
Stroop interference no. correct	17.3 (17.5)	19.8 (9.8)	12.6 (11.1)	0.53
Visuospatial				
Modified Rey copy (/17)	11.3 (5.1)	13.8 (3.6)	6.3 (4.8)	0.002
VOSP number location (/10)	6.8 (2.9)	8.9 (1.7)	4.0 (2.0)	0.001
Calculations				
Arithmetic, written (/5)	3.4 (1.3)	3.2 (0.6)	2.4 (1.5)	0.09
CATS				
Face matching (/12)	11.2 (1.3)	11.6 (0.5)	9.1 (2.0)	0.001
Affect naming (/16)	11.0 (3.0)	12.8 (2.5)	11.9 (0.9)	0.29

Shown are means (standard deviations). MMSE based on 16 patients with early-onset Alzheimer's disease, 11 patients with logopenic variant PPA and 13 patients with posterior cortical atrophy (different to Table 1).
a one-way analysis of variance across groups.
CATS = Comprehensive Affect Testing System; CVLT-SF = California Verbal Learning Test-San Francisco; EOAD = early-onset Alzheimer's disease; lvPPA = logopenic variant PPA; PCA = posterior cortical atrophy; VOSP = Visual Object and Space Perception battery.
Missing data.
Rey Figure: two posterior cortical atrophy.
Syntax comprehension: two posterior cortical atrophy.
Digit Span Forward: nine early-onset Alzheimer's disease, three logopenic variant PPA, six posterior cortical atrophy.
Digit Span Backward: one early-onset Alzheimer's disease.
Modified Trails: five early-onset Alzheimer's disease, one logopenic variant PPA, four posterior cortical atrophy.
Stroop: five early-onset Alzheimer's disease, two logopenic variant PPA, four posterior cortical atrophy.
VOSP Number Location: one early-onset Alzheimer's disease, one logopenic variant PPA, five posterior cortical atrophy.
Arithmetic: one posterior cortical atrophy.
CATS face matching: five early-onset Alzheimer's disease, two logopenic variant PPA, three posterior cortical atrophy.
CATS affect naming: five early-onset Alzheimer's disease, two logopenic variant PPA, six posterior cortical atrophy.

naming may not be the most prominent deficit in logopenic variant PPA (Gorno-Tempini *et al.*, 2004). No significant differences were found on tests of executive functioning, possibly owing to the relatively heterogeneous composition of the early-onset Alzheimer's disease group (including amnestic and dysexecutive patients) and the relatively low performance on these tasks in the group with posterior cortical atrophy owing to the high visual demand of these tests.

Voxel-wise group comparisons

Fluorodeoxyglucose-positron emission tomography results

Compared with control subjects, all three Alzheimer's disease groups showed syndrome-specific patterns of glucose hypometabolism (Fig. 1). Although all Alzheimer's disease groups showed hypometabolism in temporoparietal regions, including the angular gyrus, inferior parietal lobe, posterior cingulate/precuneus and middle and inferior temporal lobe, the involvement of these regions was asymmetric (left > right) in logopenic variant PPA and extended more posteriorly into the occipital lobes bilaterally in the group with posterior cortical atrophy. Significantly lower glucose metabolism was also found in inferior and superior frontal regions bilaterally in early-onset Alzheimer's disease, on the left in logopenic variant PPA, and on the right in posterior cortical atrophy. The early-onset Alzheimer's disease group also showed reduced metabolism in the hippocampus, in particular in the right hemisphere.

In the direct patient group comparison, patients with posterior cortical atrophy showed greater hypometabolism in lateral occipital regions compared with patients with early-onset Alzheimer's disease (Fig. 2A) and logopenic variant PPA where differences extended into the right superior parietal lobule (Fig. 2B). The group with early-onset Alzheimer's disease showed reduced metabolism in a small region in the right posterior cingulate gyrus/retrosplenial cortex compared with logopenic variant PPA (Fig. 2C). None of the other between-patient group comparisons were significant after multiple comparison correction. Similar results were found after correcting for MMSE and after atrophy correction, although the spatial extent of between group differences was more restricted on the atrophy-corrected maps (data not shown).

Pittsburgh compound B-positron emission tomography results

Compared with control subjects, all three patient groups showed diffuse patterns of higher PIB uptake across the cortex symmetrically in both hemispheres, with some sparing of the sensorimotor strip, parts of the striate cortex and the medial temporal lobes (Fig. 1). In the direct patient group comparisons, patients with posterior cortical atrophy showed higher PIB uptake in the right posterior lingual gyrus compared with patients with early-onset Alzheimer's disease (Fig. 2D), with no significant differences after FWE correction found for any of the other patient group comparisons. Relaxing the statistical threshold to $P < 0.001$, uncorrected did not return any additional differences, with the exception of lower PIB in the lingual gyrus in logopenic variant PPA compared with early-onset Alzheimer's disease. Neither MMSE correction nor atrophy correction had a substantial impact on the results, although the statistical significance of the differences was greater in the atrophy-corrected than the non-atrophy corrected comparisons (data not shown).

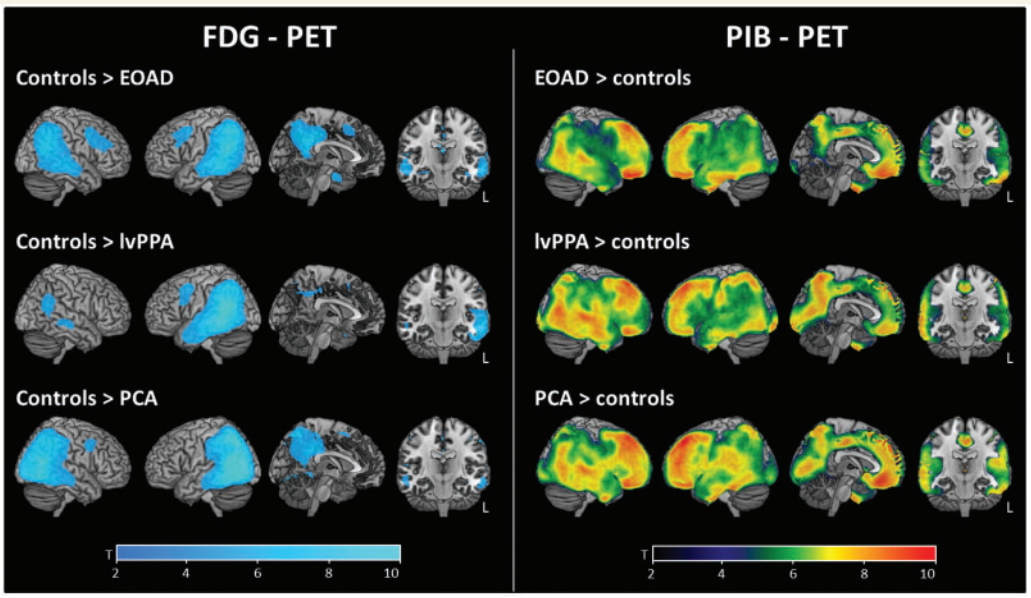

Figure 1 Patterns of FDG and PIB binding in early-onset Alzheimer's disease (EOAD), logopenic variant PPA (lvPPA) and posterior cortical atrophy (PCA) compared with healthy controls. Shown are T-maps after correction for multiple comparisons (FWE at $P < 0.05$) rendered on the ch2 template brain. Blue in the FDG maps indicates significantly lower FDG uptake in the patient groups compared with controls, whereas warmer colours in the PIB maps indicate significantly greater PIB binding in the patient groups.

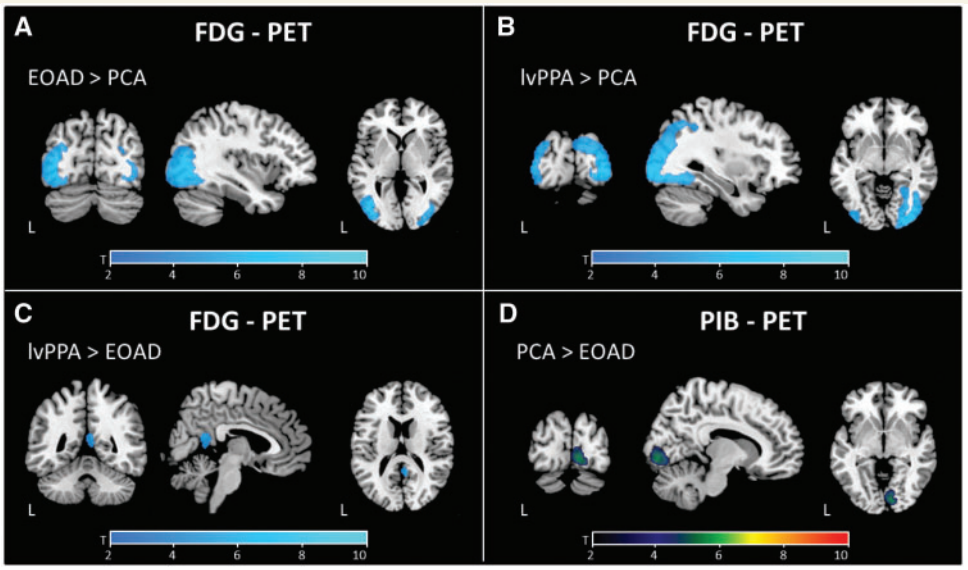

Figure 2 Differences in FDG uptake between (**A**) early-onset Alzheimer's disease (EOAD) and posterior cortical atrophy (PCA), (**B**) logopenic variant PPA (lvPPA) and posterior cortical atrophy, (**C**) logopenic variant PPA and early-onset Alzheimer's disease, and (**D**) PIB uptake in posterior cortical atrophy compared with early-onset Alzheimer's disease. Shown are T-maps after correction for multiple comparisons (FWE at $P < 0.05$) rendered on the ch2 template brain. Blue in the FDG maps indicates less FDG uptake in posterior cortical atrophy compared with early-onset Alzheimer's disease and logopenic variant PPA, and in early-onset Alzheimer's disease compared with logopenic variant PPA. Warmer colours in the PIB map indicate significantly more PIB binding in posterior cortical atrophy compared with early-onset Alzheimer's disease. Between-patient group comparisons not shown did not return statistically significant differences after FWE-correction.

Region of interest covariance analysis

Voxel-wise correlation analysis

Correlating FDG in the three seed regions of interest with FDG across the brain produced distinct patterns of covariance across patients with Alzheimer's disease (Fig. 3). There was only 7% overlap of any two correlation maps, with no regions where all three covariance maps overlapped. The regions involved for each seed region of interest showed a remarkable resemblance to specific functional networks. The results of the goodness of fit analysis for each region of interest covariance map with the best fitting network are shown in Table 3. Overlap maps of each region of interest covariance map with the best fitting network template are shown in Fig. 4. Correlation patterns for FDG with the early-onset Alzheimer's disease seed region of interest showed the best fit with the right executive-control network, mainly involving right dorsolateral prefrontal and lateral parietal regions. The correlation patterns for FDG with the logopenic variant PPA seed region of interest showed the best fit with the left language network, involving predominantly left lateral temporoparietal regions. Finally, the FDG correlation map for the posterior cortical atrophy seed region of interest showed the best fit with the higher visual network template, mainly involving bilateral occipitoparietal regions. Notably, goodness of fit scores expressed as the ratio between z_{inside} and $z_{outside}$ (Table 3) were relatively high, indicating a large difference between z_{inside} and $z_{outside}$, which, together with the overlap maps shown in Fig. 4, suggests that the best-fitting networks are specific to the corresponding region of interest correlation map.

In contrast, PIB uptake in the three seed regions of interest produced relatively diffuse covariance maps (Fig. 3), with 66% overlap of any two correlation maps and 8% of all three maps. Interestingly, PIB uptake in the posterior cortical atrophy seed region of interest (right middle occipital) showed a more focal correlation pattern that included bilateral (right more than left) medial and lateral occipital lobe regions, and left middle temporal and inferior frontal cortex. Assessing the goodness of fit of the PIB correlation maps with functional network (see Fig. 4 for the overlap with best-fit network template) revealed that, again, the logopenic variant PPA and posterior cortical atrophy correlation maps showed the best fit with the left language and higher visual networks, respectively, whereas the early-onset Alzheimer's disease region of interest correlation map showed the highest fit with the auditory network template. However, as indicated by the overlap maps in Fig. 4 and the low $z_{inside}/z_{outside}$ ratios (Table 3), the best-fitting networks were relatively non-specific to each corresponding covariance map. Similar results for both FDG and PIB correlations were found after correcting for diagnosis (Supplementary Fig. 2) and atrophy (data not shown). Testing the goodness of fit against a second, independent set of network templates (1000 Functional Connectomes Project templates) revealed similar results for both FDG and PIB, indicating that the overlap of the region of interest correlation maps with the functional network templates is robust (Supplementary Tables 1 and 2, Supplementary Figs 3 and 4).

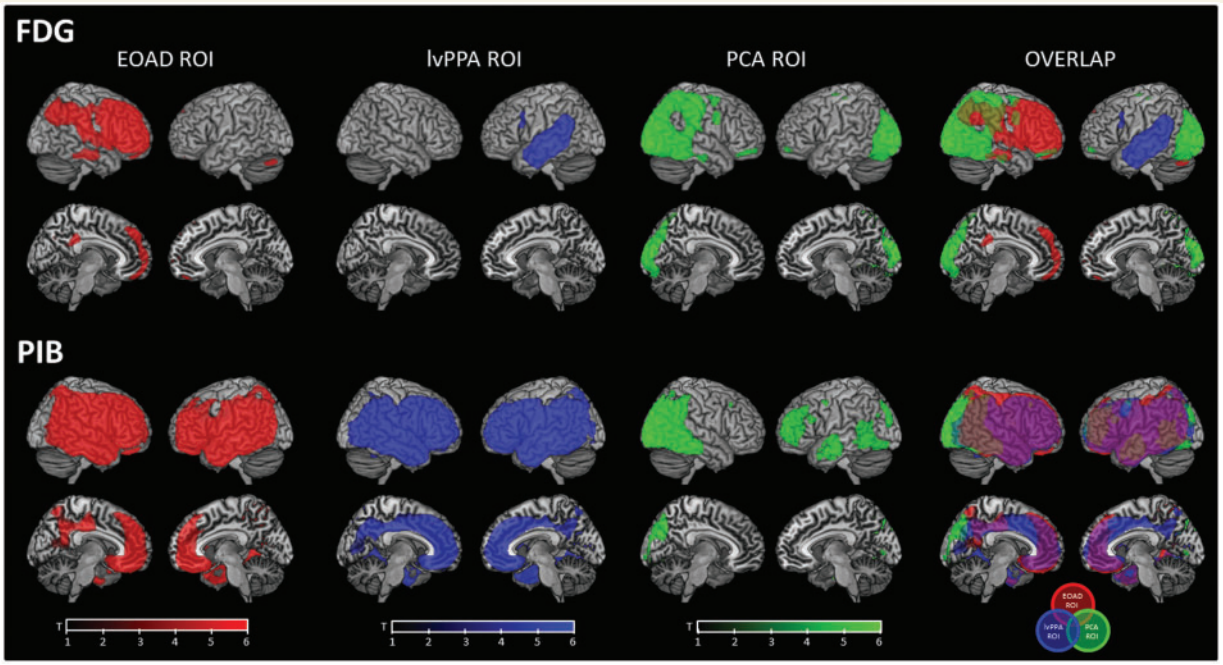

Figure 3 Region of interest (ROI) correlation maps for FDG (*top*) and PIB (*bottom*). Shown are T-values after multiple comparisons correction (FWE at $P < 0.05$) rendered on the ch2 template brain. Red maps show correlations with the early-onset Alzheimer's disease (EOAD) seed region of interest (right middle frontal gyrus); blue maps show correlations with the logopenic variant PPA (lvPPA) seed region of interest (left superior temporal sulcus); green maps show correlations with the posterior cortical atrophy (PCA) seed region of interest (right middle occipital gyrus). The overlap map shows the overlap of all three correlation maps for each tracer.

Table 3 Results of goodness of fit analysis of region of interest covariance maps with functional network templates

Correlation map	Network template with best fit	Mean z-score inside network (z_{inside})	Mean z-score outside network ($z_{outside}$)	GOF score ($z_{inside} - z_{outside}$)	Ratio ($z_{inside}/z_{outside}$)
FDG					
EOAD seed	Right executive-control	3.11	0.36	2.75	8.64
lvPPA seed	Left language	4.08	0.18	3.9	22.67
PCA seed	Higher visual	10.78	1.07	9.71	10.07
PIB					
EOAD seed	Auditory	7.52	2.47	5.05	3.04
lvPPA seed	Left language	7.95	3.24	4.71	2.45
PCA seed	Higher visual	4.97	0.66	4.31	7.53

Z_{inside} and $z_{outside}$ represent mean *z*-scores of all voxels of the region of interest correlation map that lie inside and outside the network template. The goodness of fit score represents the difference between z_{inside} and $z_{outside}$, whereas the ratio represents the ratio between z_{inside} and $z_{outside}$. The greater the difference scores and ratios, the better the fit between the correlation map and functional network.
EOAD = early-onset Alzheimer's disease; lvPPA = logopenic variant PPA; GOF = goodness of fit; PCA = posterior cortical atrophy.

Fluorodeoxyglucose and Pittsburgh compound B uptake in functional network templates

Mean FDG and PIB values for the five functional networks examined for each group are illustrated in Fig. 5. Compared with controls, all Alzheimer's disease variants showed significantly lower FDG and higher PIB uptake in all networks ($P < 0.0001$). Between Alzheimer's disease clinical variants, no differences were found in the dorsal default mode network, indicating that FDG was similarly reduced in all three groups. Although patients with logopenic variant PPA showed higher FDG in the ventral default mode network ($P = 0.01$ compared with early-onset Alzheimer's disease, $P = 0.003$ compared with posterior cortical atrophy), this was driven by relative sparing of this network in the right hemisphere in this group. Splitting the ventral default mode network into left and right-sided components revealed higher FDG uptake in the right ($P < 0.001$) but not left ventral default mode network ($P = 0.26$). FDG uptake was also higher in the logopenic variant PPA group in the right executive-control network ($P = 0.02$

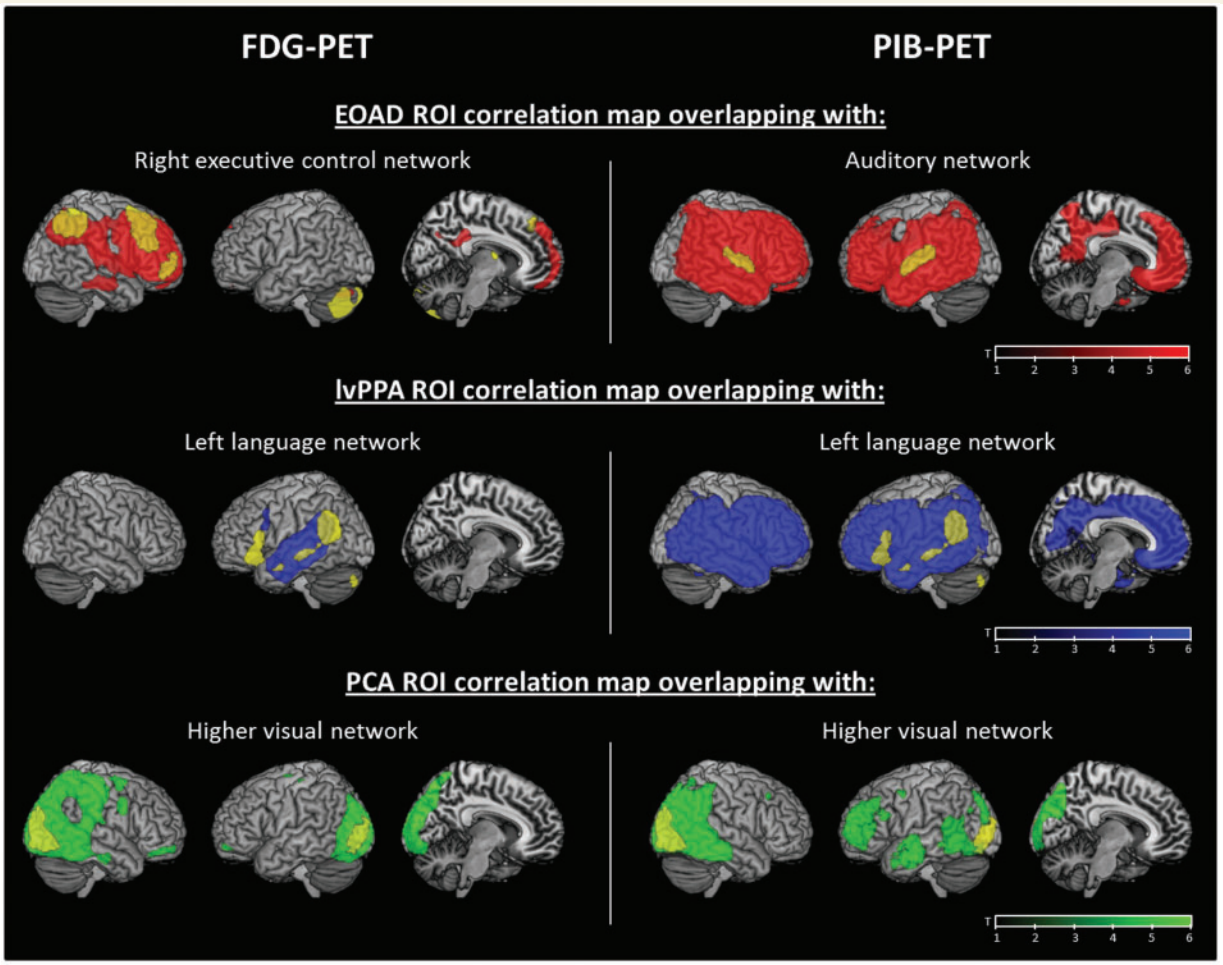

Figure 4 Overlap maps showing each region of interest (ROI) correlation map with the best-fitting network template (i.e. network with highest goodness-of-fit score) for FDG and PIB. Red, blue and green maps represent T-values for significant (FWE $P < 0.05$) correlations with the respective seed regions of interest for early-onset Alzheimer's disease (EOAD), logopenic variant PPA (lvPPA) and posterior cortical atrophy (PCA), respectively, whereas yellow represents the corresponding network template.

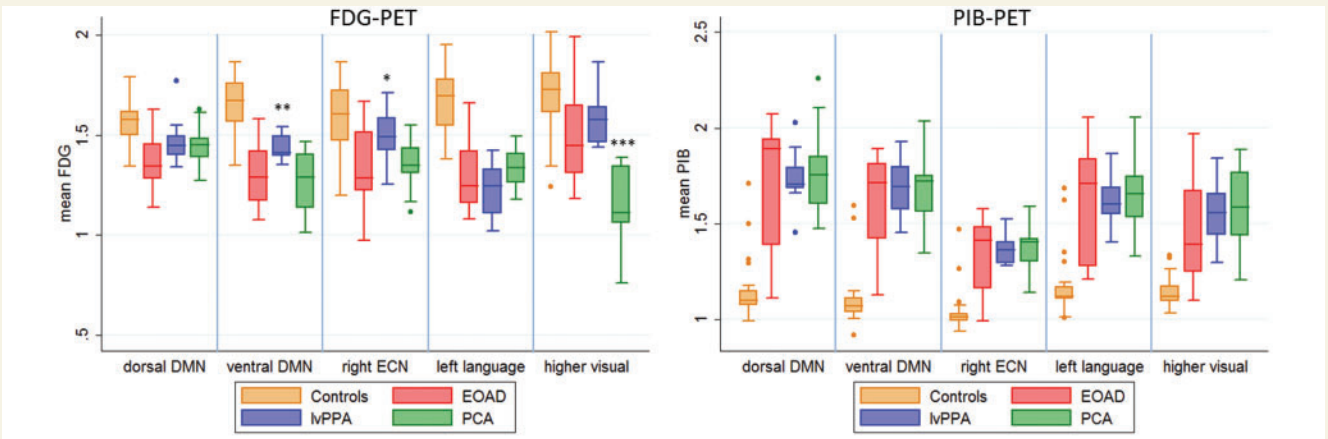

Figure 5 Mean FDG and PIB values for each group and the functional network templates. All Alzheimer's disease groups showed significantly lower FDG and higher PIB compared with controls. Asterisk denote FDG in logopenic variant PPA significantly higher than in early-onset Alzheimer's disease and posterior cortical atrophy $P < 0.05$; double asterisk denotes FDG in logopenic variant PPA significantly higher than in early-onset Alzheimer's disease and posterior cortical atrophy $P < 0.01$; triple asterisks denote FDG in posterior cortical atrophy significantly lower than in early-onset Alzheimer's disease and logopenic variant PPA $P < 0.0001$. DMN = default mode network; ECN = executive-control network.

compared with early-onset Alzheimer's disease, $P = 0.04$ compared with posterior cortical atrophy), whereas the posterior cortical atrophy group showed lower FDG in the higher visual network ($P < 0.0001$). A trend for lower FDG in the left language network was also found in logopenic variant PPA compared with posterior cortical atrophy on pairwise comparison ($P = 0.08$). Notably, within each Alzheimer's disease group, patients with early-onset Alzheimer's disease showed greatest reduction in FDG in the left executive-control network, whereas the logopenic variant PPA group showed greatest hypometabolism in the left language network, and the posterior cortical atrophy group in the higher visual network. PIB uptake did not differ between Alzheimer's disease groups in any of the networks ($P > 0.27$).

Discussion

This is the first study to directly compare glucose metabolism and amyloid deposition patterns *in vivo* across three clinical variants of early age-of-onset Alzheimer's disease: early-onset Alzheimer's disease, logopenic variant PPA and posterior cortical atrophy. These less common focal variants of Alzheimer's disease were chosen to maximize heterogeneity in our study population and increase the likelihood of identifying mechanisms that contribute to the clinico-anatomic variance of the disease. We hypothesized that Alzheimer's disease syndromes would be characterized by focal patterns of hypometabolism (FDG-PET), which would closely mirror specific functional networks and would not be explained by patterns of amyloid deposition (PIB-PET). We further predicted that the default mode network would be involved in all three Alzheimer's disease variants, whereas the involvement of the executive-control, language and visual networks would be specific to early-onset Alzheimer's disease, logopenic variant PPA and posterior cortical atrophy, respectively. Using a traditional mass-univariate voxel-wise comparison approach, we found syndrome-specific patterns of hypometabolism in all three Alzheimer's disease variants compared with control subjects, whereas PIB retention was widespread across association neocortex. The seed region of interest covariance analysis revealed distinct, syndrome-specific FDG covariance patterns that greatly overlapped with the predicted functional networks, whereas PIB correlation maps were diffuse and largely overlapping. Finally, assessing FDG and PIB uptake in functional network templates revealed significantly lower FDG and higher PIB in the Alzheimer's disease variants compared with control subjects in all networks. Although FDG uptake was similarly reduced across all variants in the dorsal and left ventral default mode network, significant differences between Alzheimer's disease variants were found in the right ventral default mode network, right executive-control and higher visual networks, with a trend towards lower FDG also found in the left language network in logopenic variant PPA. In contrast, PIB uptake did not differ between Alzheimer's disease variants in any of the networks. Together, these findings suggest that clinical variants of Alzheimer's disease are characterized by differential involvement of specific functional networks, whereas the dorsal default mode network is commonly affected in all variants. Our results also suggest that fibrillar amyloid-β deposition explains at most a small amount of the clinico-anatomical heterogeneity in Alzheimer's disease.

Our three FDG analyses provide converging evidence implicating differential involvement of specific networks in each clinical variant of Alzheimer's disease. Perhaps the most distinct pattern was found in posterior cortical atrophy, where on voxel-wise group comparisons, we found greater involvement of lateral occipital and posterior inferior temporal regions. Patients with posterior cortical atrophy showed lower FDG uptake than other variants in the higher-order visual network template, and showed the most dramatic overlap between the seed region of interest correlation map (focused in right middle occipital gyrus) and the higher-order visual network template. Consistent with previous reports (Rabinovici *et al.*, 2008; Josephs *et al.*, 2010), patients with logopenic variant PPA showed hypometabolism in left temporoparietal cortex that was far more asymmetric than the pattern seen in early-onset Alzheimer's disease. The region of interest correlation map (seeded by the left superior temporal gyrus) best fit the left language network template. On voxel-wise comparisons, patients with early-onset Alzheimer's disease showed greater involvement of the hippocampus (versus control subjects) and retrosplenial cortex (versus logopenic variant PPA), and low FDG uptake in the ventral default mode network. Patients with early-onset Alzheimer's disease further demonstrated low FDG in the right executive-control network, and the region of interest correlation map (focused in right middle frontal gyrus) demonstrated a best fit with this network. These findings match the clinical profile of patients with early-onset Alzheimer's disease, which includes amnestic and dysexecutive deficits. Interestingly, our region of interest correlation maps were not altered when clinical group was added as a covariate, suggesting that these correlation maps are not driven by each of the variants, but are capturing involvement of networks across all subjects with Alzheimer's disease.

In addition to metabolic differences, we also found significant overlap in FDG patterns across Alzheimer's disease phenotypes. This was most notable in the dorsal default mode network, where FDG uptake was similarly reduced across all variants, suggesting that the involvement of this network is a common feature of Alzheimer's disease, irrespective of clinical phenotype (Lehmann *et al.*, 2010; Whitwell *et al.*, 2011). Although there was a significant difference in FDG uptake in the ventral default mode network, this was driven by the asymmetric pattern of logopenic variant PPA, as a *post hoc* analysis that split the ventral default mode network into left and right components revealed that FDG uptake in the left ventral default mode network was as low in logopenic variant PPA as in early-onset Alzheimer's disease and posterior cortical atrophy. Additional overlap occurred in the right executive-control network in all but the logopenic variant PPA variant, and also in the language network, although a trend towards lower FDG uptake was found in logopenic variant PPA. Overlapping involvement of these networks is consistent with the observation that clinically defined Alzheimer's disease variants show some degree of behavioural and anatomical overlap at baseline that increases with longitudinal evolution (Migliaccio *et al.*, 2009; Lehmann *et al.*, 2012).

In striking contrast to the syndrome-specific FDG patterns, PIB binding was diffuse across clinical syndromes and between networks. Perhaps the one exception to this rule was posterior cortical atrophy, where we found increased PIB uptake in the right posterior lingual gyrus in posterior cortical atrophy compared with early-onset Alzheimer's disease. This finding stands in contrast to other group imaging studies that have found no significant differences in PIB retention between posterior cortical atrophy and typical Alzheimer's disease (Rosenbloom *et al.*, 2010; de Souza *et al.*, 2011), although trends towards higher PIB uptake in cuneus and lingual regions of interest were found after atrophy correction in Rosenbloom *et al*. (2010). Reasons for discrepant findings between this and other PIB group studies may include differences in sample size, group composition (e.g. early-onset Alzheimer's disease versus typical Alzheimer's disease that may include cases with late-onset Alzheimer's disease) and methodological differences (e.g. different versions of SPM). However, even in posterior cortical atrophy, there was a marked dissociation between the largely overlapping PIB binding patterns and the very distinct hypometabolic pattern seen on voxel-wise contrasts and in interrogating the higher-order visual network. Interestingly, the PIB covariance pattern of the posterior cortical atrophy (right occipital) seed region of interest was also the most focal, raising the possibility that occipital PIB binding is capturing a more distinct process. Autopsy and PIB studies have suggested that cerebral amyloid angiopathy is particularly prominent in the occipital lobe (Rosand *et al.*, 2005; Johnson *et al.*, 2007; Ly *et al.*, 2010), raising the possibility that cerebral amyloid angiopathy contributes to the strong occipital PIB signal in Alzheimer's disease. Further studies are needed to assess the prevalence of cerebral amyloid angiopathy in Alzheimer's disease and its contribution to the neurodegenerative patterns found in different Alzheimer's disease syndromes.

If amyloid-β aggregation is the initiating event in the Alzheimer's disease cascade, how can we reconcile the diffuse patterns of amyloid deposition with the network-specific patterns of neurodegeneration seen in Alzheimer's disease variants? One possibility is to consider that amyloid-β and tau aggregation may be driven by distinct mechanisms, with neurofibrillary rather than amyloid pathology driving neurodegeneration. Studies have shown that amyloid-β secretion and local aggregation in mouse models correlate with neural activity (Cirrito *et al.*, 2005; Bero *et al.*, 2011), and that amyloid-β accumulation in humans occurs in highly interconnected cortical hubs (Buckner *et al.*, 2009), even in preclinical stages (Mintun *et al.*, 2006; Fripp *et al.*, 2008; Mormino *et al.*, 2011). Cortical hubs are distributed across wide regions of association neocortex, leading to diffuse and symmetric patterns of amyloid-β aggregation that are not confined to specific networks. Interestingly, recent *in vitro* (Frost *et al.*, 2009; Nonaka *et al.*, 2010; Guo and Lee, 2011) and *in vivo* findings in transgenic mice (Clavaguera *et al.*, 2009; de Calignon *et al.*, 2012) have found that misfolding and aggregation of tau may spread via synaptic connections, therefore leading to the progression of disease within specific interconnected neural networks. If relevant to human disease, these observations suggest that the aggregation of amyloid-β may be driven by total flow of neuronal activity (yielding diffuse and symmetric patterns of PIB binding throughout 'cortical hubs'), whereas the aggregation of tau may be driven by transneuronal spread, generating patterns of neurodegeneration that coincide with specific functional networks and ultimately lead to specific clinical phenotypes.

Although speculative, this model would account for the exquisitely specific regional patterns of neurodegeneration seen in early stages of Alzheimer's disease (Reiman *et al.*, 1996; Petrie *et al.*, 2009), which contrasts with the diffuse pattern of amyloid deposition. This model could also explain the central role of the default mode network in Alzheimer's disease, as the default mode network may represent a network in which early amyloid-β aggregation (as a central hub) and metabolic vulnerability (Liang *et al.*, 2008) converge. Trans-synaptic spread could explain how the disease spreads from the default mode network to closely interconnected posterior networks, including those involved in visuospatial, language and executive function. There is currently limited data on the direction of the transneuronal spread, i.e. it is possible that Alzheimer's disease pathology begins in different 'off-target' networks in Alzheimer's disease variants that later converge in the default mode network. Further studies using longitudinal data will provide insights into the chain of events in different Alzheimer's disease variants.

The centrality of tau pathology to clinical symptoms is consistent with the vast majority of clinicopathological studies that have found that tangle pathology is a better predictor of neurodegeneration, disease severity and cognitive symptoms in Alzheimer's disease than amyloid pathology (see Nelson *et al.*, 2012 for a review). Autopsy studies have also shown greater tangle, but not amyloid pathology in posterior regions in posterior cortical atrophy (Renner *et al.*, 2004; Tang-Wai *et al.*, 2004) and in left hemisphere language regions in PPA versus amnestic Alzheimer's disease (Mesulam *et al.*, 2008; Gefen *et al.*, 2012). The regions with greatest tangle pathology, therefore, greatly overlap with the most atrophied and hypometabolic regions in these different syndromes, suggesting good correspondence between the distribution of tau and patterns of neurodegeneration. The factors that drive neurofibrillary pathology into specific, distinct brain networks in individuals with Alzheimer's disease are largely unknown. Genetic association studies suggest that the ApoE ε4 allele and perhaps specific tau haplotypes may drive neurofibrillary pathology into the medial temporal lobe and hippocampus (Murray *et al.*, 2011; van der Flier *et al.*, 2011; similar trend for a higher prevalence of ε4 alleles in early-onset Alzheimer's disease in our study), whereas the high rate of developmental language disorders in patients with PPA hints at premorbid developmental vulnerability as a potential mechanism (Rogalski *et al.*, 2008). It is likely that many more genetic and environmental risk factors (as well as interactions between the two) that have yet to be elucidated are involved in determining the pattern of neurodegeneration in Alzheimer's disease.

It is also conceivable that distinct clinico-anatomical features in Alzheimer's disease variants may be driven by amyloid species that are not captured by PIB, such as soluble amyloid-β or diffuse plaques (Bacskai *et al.*, 2007; Ikonomovic *et al.*, 2008). In particular, amyloid-β oligomers, which are considered the most neurotoxic of all amyloid species (Mucke *et al.*, 2000; Walsh and Selkoe, 2007), may significantly contribute to different neurodegenerative patterns in Alzheimer's disease. Additionally, we cannot exclude

the possibility that Alzheimer's disease variants may show focal or asymmetric patterns of amyloid deposition in preclinical stages of Alzheimer's disease. Although the pattern of PIB binding in amyloid-positive cognitively normal individuals appears relatively diffuse at a group level (Mintun *et al.*, 2006; Fripp *et al.*, 2008; Mormino *et al.*, 2012), focal patterns can be seen in individual cases, and these may be relevant to the subsequent pattern of neurodegeneration. Interestingly, our PIB covariance analysis showed best goodness of fit between the logopenic variant PPA region of interest covariance map and the left language network, and between the posterior cortical atrophy region of interest map and the higher-order visual network. However, the PIB goodness of fit findings should be interpreted with caution, as the high number of other fits with similar goodness of fit scores suggests that the best-fit network is relatively non-specific.

Our study has limitations. Autopsy confirmation of Alzheimer's disease is not available in any of our subjects, though our selection criteria were designed to maximize the likelihood of underlying Alzheimer's disease pathology (clinical phenotypes highly associated with post-mortem Alzheimer's disease, exclusion of patients with core features of other degenerative diseases, required evidence of amyloid deposition on PIB-PET scans). Although the sample size of the different Alzheimer's disease groups in this study is relatively large, given the frequency of the syndromes, subject numbers may have been too small to detect significant differences in PIB retention between Alzheimer's disease variants, although sample sizes were large enough to detect differences in FDG. Our choice of an early age-of-onset Alzheimer's disease group controlled for the effects of age (as logopenic variant PPA and posterior cortical atrophy typically occur in early-onset patients) and enhanced comparisons with a previous structural imaging study (Migliaccio *et al.*, 2009). However, this may have limited our ability to detect behavioural and imaging differences between 'typical' Alzheimer's disease and logopenic variant PPA/posterior cortical atrophy, as patients with early-onset Alzheimer's disease show early language and visuospatial deficits (Koss *et al.*, 1996; Koedam *et al.*, 2010). Although the late-onset amnestic Alzheimer's disease phenotype is more common than the early-onset variants, using these variants to study the factors driving clinical heterogeneity provides important insights into disease pathogenesis that may be applicable to the more common, late-onset Alzheimer's disease. PIB, although a highly validated tracer, is relatively novel and may have unknown limitations (e.g. ceiling effects or unknown binding interactions). A further point of ongoing debate is the potential confounding effects of atrophy on PIB data. Reassuringly our results were consistent with and without atrophy correction. MRI scans were acquired on different scanners. However, patient groups were relatively matched for scanner type, and the use of structural imaging in this study was limited to definition of regions of interest, spatial normalization and atrophy correction of PET data. Finally, although FDG-PET is closely related to synaptic activity (Jueptner and Weiller, 1995) and has been widely used to assess brain function, it is an indirect method of identifying functional neural networks. Future studies applying both task-free and task-dependent functional MRI data may help to confirm and further elucidate the role of different functional networks in Alzheimer's disease variants.

Acknowledgements

The authors would like to acknowledge Baber Khan and Teresa Wu for administrative support, and Andrea Long for assistance with PET scanning.

Funding

Alzheimer's Research UK grant (to M.L.); National Institute on Aging grants [K23-AG031861] (to G.D.R.), [R01-AG027859] (to W.J.J.), [P01-AG1972403 and P50-AG023501] (to B.L.M.), [RO1NS073498] (to M.D.G.); Alzheimer's Association grants [NIRG-07-59422] (to G.D.R.) and [ZEN-08-87090] (to W.J.J.); John Douglas French Alzheimer's Foundation (to G.D.R.); State of California Department of Health Services Alzheimer's Disease Research Centre of California grant [04-33516] (to B.L.M); and Hellman Family Foundation (to G.D.R.).

Supplementary material

Supplementary material is available at *Brain* online.

References

Bacskai BJ, Frosch MP, Freeman SH, Raymond SB, Augustinack JC, Johnson KA, et al. Molecular imaging with Pittsburgh compound B confirmed at autopsy—a case report. Arch Neurol 2007; 64: 431–4.

Benson F, Davis J, Snyder BD. Posterior cortical atrophy. Arch Neurol 1988; 45: 789–93.

Bero AW, Yan P, Roh JH, Cirrito JR, Stewart FR, Raichle ME, et al. Neuronal activity regulates the regional vulnerability to amyloid-beta deposition. Nat Neurosci 2011; 14: 750–6.

Biswal BB, Mennes M, Zuo XN, Gohel S, Kelly C, Smith SM, et al. Toward discovery science of human brain function. Proc Natl Acad Sci U S A 2010; 107: 4734–4739.

Buckner RL, Sepulcre J, Talukdar T, Krienen FM, Liu H, Hedden T, et al. Cortical hubs revealed by intrinsic functional connectivity: mapping, assessment of stability, and relation to Alzheimer's disease. J Neurosci 2009; 29: 1860–73.

Cirrito JR, Yamada KA, Finn MB, Sloviter RS, Bales KR, May PC, et al. Synaptic activity regulates interstitial fluid amyloid-beta levels in vivo. Neuron 2005; 48: 913–22.

Clavaguera F, Bolmont T, Crowther RA, Abramowski D, Frank S, Probst A, et al. Transmission and spreading of tauopathy in transgenic mouse brain. Nat Cell Biol 2009; 11: 909–13.

Crutch SJ, Lehmann M, Schott JM, Rabinovici GD, Rossor MN, Fox NC. Posterior cortical atrophy. Lancet Neurol 2012; 11: 170–8.

Dale AM, Fischl B, Sereno MI. Cortical surface-based analysis—I. Segmentation and surface reconstruction. Neuroimage 1999; 9: 179–94.

de Calignon A, Polydoro M, Suarez-Calvet M, William C, Adamowicz DH, Kopeikina KJ, et al. Propagation of tau pathology in a model of early Alzheimer's disease. Neuron 2012; 73: 685–97.

de Souza LC, Corlier F, Habert MO, Uspenskaya O, Maroy R, Lamari F, et al. Similar amyloid-{beta} burden in posterior cortical atrophy and Alzheimer's disease. Brain 2011; 134 (Pt 7): 2036–43.

Folstein MF, Folstein SE, McHugh PR. Mini-mental state - Practical method for grading cognitive state of patients for clinician. J Psychiatr Res 1975; 12: 189–98.

Formaglio M, Costes N, Seguin J, Tholance Y, Le BD, Roullet-Solignac I, et al. In vivo demonstration of amyloid burden in posterior cortical atrophy: a case series with PET and CSF findings. J Neurol 2011; 258: 1841–51.

Fripp J, Bourgeat P, Acosta O, Raniga P, Modat M, Pike KE, et al. Appearance modeling of 11C PiB PET images: characterizing amyloid deposition in Alzheimer's disease, mild cognitive impairment and healthy aging. Neuroimage 2008; 43: 430–9.

Frisoni GB, Pievani M, Testa C, Sabattoli F, Bresciani L, Bonetti M, et al. The topography of grey matter involvement in early and late onset Alzheimer's disease. Brain 2007; 130: 720–30.

Frisoni GB, Testa C, Sabattoli F, Beltramello A, Soininen H, Laakso MP. Structural correlates of early and late onset Alzheimer's disease: voxel based morphometric study. J Neurol Neurosurg Psychiatry 2005; 76: 112–14.

Frost B, Jacks RL, Diamond MI. Propagation of tau misfolding from the outside to the inside of a cell. J Biol Chem 2009; 284: 12845–52.

Galton CJ, Patterson K, Xuereb JH, Hodges JR. Atypical and typical presentations of Alzheimer's disease: a clinical, neuropsychological, neuroimaging and pathological study of 13 cases. Brain 2000; 123: 484–98.

Gefen T, Gasho K, Rademaker A, Lalehzari M, Weintraub S, Rogalski E, et al. Clinically concordant variations of Alzheimer pathology in aphasic versus amnestic dementia. Brain 2012; 135: 1554–65.

Gorno-Tempini ML, Brambati SM, Ginex V, Ogar J, Dronkers NF, Marcone A, et al. The logopenic/phonological variant of primary progressive aphasia. Neurology 2008; 71: 1227–34.

Gorno-Tempini ML, Dronkers NF, Rankin KP, Ogar JM, Phengrasamy L, Rosen HJ, et al. Cognition and anatomy in three variants of primary progressive aphasia. Ann Neurol 2004; 55: 335–46.

Gorno-Tempini ML, Hillis AE, Weintraub S, Kertesz A, Mendez M, Cappa SF, et al. Classification of primary progressive aphasia and its variants. Neurology 2011; 76: 1006–14.

Grady CL, Springer MV, Hongwanishkul D, McIntosh AR, Winocur G. Age-related changes in brain activity across the adult lifespan. J Cogn Neurosci 2006; 18: 227–41.

Greicius MD, Srivastava G, Reiss AL, Menon V. Default-mode network activity distinguishes Alzheimer's disease from healthy aging: evidence from functional MRI. Proc Natl Acad Sci USA 2004; 101: 4637–42.

Greicius MD, Supekar K, Menon V, Dougherty RF. Resting-state functional connectivity reflects structural connectivity in the default mode network. Cereb Cortex 2009; 19: 72–8.

Guo JL, Lee VM. Seeding of normal Tau by pathological Tau conformers drives pathogenesis of Alzheimer-like tangles. J Biol Chem 2011; 286: 15317–31.

Hampson M, Peterson BS, Skudlarski P, Gatenby JC, Gore JC. Detection of functional connectivity using temporal correlations in MR images. Hum Brain Mapp 2002; 15: 247–62.

Hof PR, Vogt BA, Bouras C, Morrison JH. Atypical form of Alzheimer's disease with prominent posterior cortical atrophy: a review of lesion distribution and circuit disconnection in cortical visual pathways. Vision Res 1997; 37: 3609–25.

Holmes C, Boche D, Wilkinson D, Yadegarfar G, Hopkins V, Bayer A, et al. Long-term effects of Abeta42 immunisation in Alzheimer's disease: follow-up of a randomised, placebo-controlled phase I trial. Lancet 2008; 372: 216–23.

Ikonomovic MD, Klunk WE, Abrahamson EE, Mathis CA, Price JC, Tsopelas ND, et al. Post-mortem correlates of in vivo PiB-PET amyloid imaging in a typical case of Alzheimer's disease. Brain 2008; 131: 1630–45.

Johnson KA, Gregas M, Becker JA, Kinnecom C, Salat DH, Moran EK, et al. Imaging of amyloid burden and distribution in cerebral amyloid angiopathy. Ann Neurol 2007; 62: 229–34.

Josephs KA, Duffy JR, Fossett TR, Strand EA, Claassen DO, Whitwell JL, et al. Fluorodeoxyglucose F18 positron emission tomography in progressive apraxia of speech and primary progressive aphasia variants. Arch Neurol 2010; 67: 596–605.

Jueptner M, Weiller C. Review: does measurement of regional cerebral blood flow reflect synaptic activity? Implications for PET and fMRI. Neuroimage 1995; 2: 148–56.

Kambe T, Motoi Y, Ishii K, Hattori N. Posterior cortical atrophy with [C-11] Pittsburgh compound B accumulation in the primary visual cortex. J Neurol 2010; 257: 469–71.

Knibb JA, Xuereb JH, Patterson K, Hodges JR. Clinical and pathological characterization of progressive aphasia. Ann Neurol 2006; 59: 156–65.

Koedam EL, Lauffer V, van der Vlies AE, van der Flier WM, Scheltens P, Pijnenburg YA. Early-versus late-onset Alzheimer's disease: more than age alone. J Alzheimers Dis 2010; 19: 1401–8.

Koss E, Edland S, Fillenbaum G, Mohs R, Clark C, Galasko D, et al. Clinical and neuropsychological differences between patients with earlier and later onset of Alzheimer's disease: a CERAD analysis, Part XII. Neurology 1996; 46: 136–41.

Kramer JH, Jurik J, Sha SJ, Rankin KP, Rosen HJ, Johnson JK, et al. Distinctive neuropsychological patterns in frontotemporal dementia, semantic dementia, and Alzheimer disease. Cogn Behav Neurol 2003; 16: 211–8.

Lehmann M, Barnes J, Ridgway GR, Ryan NS, Warrington EK, Crutch SJ, et al. Global gray matter changes in posterior cortical atrophy: a serial imaging study. Alzheimers Dement 2012; 8: 502–12.

Lehmann M, Crutch SJ, Ridgway GR, Ridha BH, Barnes J, Warrington EK, et al. Cortical thickness and voxel-based morphometry in posterior cortical atrophy and typical Alzheimer's disease. Neurobiol Aging 2011; 32: 1466–76.

Lehmann M, Rohrer JD, Clarkson MJ, Ridgway GR, Scahill RI, Modat M, et al. Reduced cortical thickness in the posterior cingulate gyrus is characteristic of both typical and atypical Alzheimer's disease. J Alzheimers Dis 2010; 20: 587–98.

Levine DN, Lee JM, Fisher CM. The visual variant of Alzheimer's disease: a clinicopathologic case study. Neurology 1993; 43: 305–13.

Leyton CE, Villemagne VL, Savage S, Pike KE, Ballard KJ, Piguet O, et al. Subtypes of progressive aphasia: application of the International Consensus Criteria and validation using beta-amyloid imaging. Brain 2011; 134 (Pt 10): 3030–43.

Liang WS, Reiman EM, Valla J, Dunckley T, Beach TG, Grover A, et al. Alzheimer's disease is associated with reduced expression of energy metabolism genes in posterior cingulate neurons. Proc Natl Acad Sci USA 2008; 105: 4441–6.

Logan J, Fowler JS, Volkow ND, Wang GJ, Ding YS, Alexoff DL. Distribution volume ratios without blood sampling from graphical analysis of PET data. J Cereb Blood Flow Metab 1996; 16: 834–40.

Ly JV, Donnan GA, Villemagne VL, Zavala JA, Ma H, O'Keefe G, et al. 11C-PIB binding is increased in patients with cerebral amyloid angiopathy-related hemorrhage. Neurology 2010; 74: 487–93.

McKhann GM, Knopman DS, Chertkow H, Hyman BT, Jack CR Jr, Kawas CH, et al. The diagnosis of dementia due to Alzheimer's disease: recommendations from the National Institute on Aging-Alzheimer's Association workgroups on diagnostic guidelines for Alzheimer's disease. Alzheimers Dement 2011; 7: 263–9.

Meltzer CC, Leal JP, Mayberg HS, Wagner HN Jr, Frost JJ. Correction of PET data for partial volume effects in human cerebral cortex by MR imaging. J Comput Assist Tomogr 1990; 14: 561–70.

Mendez MF, Ghajarania M, Perryman KM. Posterior cortical atrophy: clinical characteristics and differences compared to Alzheimer's disease. Dement Geriatr Cogn Disord 2002; 14: 33–40.

Mesulam M, Wicklund A, Johnson N, Rogalski E, Leger GC, Rademaker A, et al. Alzheimer and frontotemporal pathology in subsets of primary progressive aphasia. Ann Neurol 2008; 63: 709–19.

Migliaccio R, Agosta F, Rascovsky K, Karydas A, Bonasera S, Rabinovici GD, et al. Clinical syndromes associated with posterior atrophy early age at onset AD spectrum. Neurology 2009; 73: 1571–8.

Miller SL, Celone K, DePeau K, Diamond E, Dickerson BC, Rentz D, et al. Age-related memory impairment associated with loss of parietal deactivation but preserved hippocampal activation. Proc Natl Acad Sci USA 2008; 105: 2181–6.

Minoshima S, Frey KA, Foster NL, Kuhl DE. Preserved pontine glucose metabolism in Alzheimer disease: a reference region for functional brain image (PET) analysis. J Comput Assist Tomogr 1995; 19: 541–7.

Mintun MA, Larossa GN, Sheline YI, Dence CS, Lee SY, Mach RH, et al. [11C]PIB in a nondemented population: potential antecedent marker of Alzheimer disease. Neurology 2006; 67: 446–52.

Mormino EC, Brandel MG, Madison CM, Rabinovici GD, Marks S, Baker SL, et al. Not quite PIB-positive, not quite PIB-negative: slight PIB elevations in elderly normal control subjects are biologically relevant. Neuroimage 2012; 59: 1152–60.

Mormino EC, Kluth JT, Madison CM, Rabinovici GD, Baker SL, Miller BL, et al. Episodic memory loss is related to hippocampal-mediated-amyloid deposition in elderly subjects. Brain 2009; 132: 1310–23.

Mormino EC, Smiljic A, Hayenga AO, Onami SH, Greicius MD, Rabinovici GD, et al. Relationships between beta-amyloid and functional connectivity in different components of the default mode network in aging. Cereb Cortex 2011; 21: 2399–407.

Mucke L, Masliah E, Yu GQ, Mallory M, Rockenstein EM, Tatsuno G, et al. High-level neuronal expression of abeta 1-42 in wild-type human amyloid protein precursor transgenic mice: synaptotoxicity without plaque formation. J Neurosci 2000; 20: 4050–8.

Mueller SG, Laxer KD, Barakos J, Cheong I, Garcia P, Weiner MW. Widespread neocortical abnormalities in temporal lobe epilepsy with and without mesial sclerosis. Neuroimage 2009; 46: 353–9.

Murray ME, Graff-Radford NR, Ross OA, Petersen RC, Duara R, Dickson DW. Neuropathologically defined subtypes of Alzheimer's disease with distinct clinical characteristics: a retrospective study. Lancet Neurol 2011; 10: 785–96.

Nelson PT, Alafuzoff I, Bigio EH, Bouras C, Braak H, Cairns NJ, et al. Correlation of Alzheimer disease neuropathologic changes with cognitive status: a review of the literature. J Neuropathol Exp Neurol 2012; 71: 362–81.

Ng SY, Villemagne VL, Masters CL, Rowe CC. Evaluating atypical dementia syndromes using positron emission tomography with carbon 11 labeled Pittsburgh Compound B. Arch Neurol 2007; 64: 1140–4.

Nonaka T, Watanabe ST, Iwatsubo T, Hasegawa M. Seeded aggregation and toxicity of {alpha}-synuclein and tau: cellular models of neurodegenerative diseases. J Biol Chem 2010; 285: 34885–98.

Otten LJ, Rugg MD. When more means less: neural activity related to unsuccessful memory encoding. Curr Biol 2001; 11: 1528–30.

Petrie EC, Cross DJ, Galasko D, Schellenberg GD, Raskind MA, Peskind ER, et al. Preclinical evidence of Alzheimer changes: convergent cerebrospinal fluid biomarker and fluorodeoxyglucose positron emission tomography findings. Arch Neurol 2009; 66: 632–7.

Price JC, Klunk WE, Lopresti BJ, Lu X, Hoge JA, Ziolko SK, et al. Kinetic modeling of amyloid binding in humans using PET imaging and Pittsburgh Compound-B. J Cereb Blood Flow Metab 2005; 25: 1528–47.

Rabinovici GD, Furst AJ, Alkalay A, Racine CA, O'Neil JP, Janabi M, et al. Increased metabolic vulnerability in early-onset Alzheimer's disease is not related to amyloid burden. Brain 2010; 133 (Pt 2): 512–28.

Rabinovici GD, Jagust WJ, Furst AJ, Ogar JM, Racine CA, Mormino EC, et al. Abeta amyloid and glucose metabolism in three variants of primary progressive aphasia. Ann Neurol 2008; 64: 388–401.

Reiman EM, Caselli RJ, Yun LS, Chen K, Bandy D, Minoshima S, et al. Preclinical evidence of Alzheimer's disease in persons homozygous for the epsilon 4 allele for apolipoprotein E. N Engl J Med 1996; 334: 752–8.

Renner JA, Burns JM, Hou CE, McKeel DW Jr, Storandt M, Morris JC. Progressive posterior cortical dysfunction: a clinicopathologic series. Neurology 2004; 63: 1175–80.

Rogalski E, Johnson N, Weintraub S, Mesulam M. Increased frequency of learning disability in patients with primary progressive aphasia and their first-degree relatives. Arch Neurol 2008; 65: 244–8.

Rombouts SA, Barkhof F, Goekoop R, Stam CJ, Scheltens P. Altered resting state networks in mild cognitive impairment and mild Alzheimer's disease: an fMRI study. Hum Brain Mapp 2005; 26: 231–9.

Rosand J, Muzikansky A, Kumar A, Wisco JJ, Smith EE, Betensky RA, et al. Spatial clustering of hemorrhages in probable cerebral amyloid angiopathy. Ann Neurol 2005; 58: 459–62.

Rosen HJ, Gorno-Tempini ML, Goldman WP, Perry RJ, Schuff N, Weiner M, et al. Patterns of brain atrophy in frontotemporal dementia and semantic dementia. Neurology 2002; 58: 198–208.

Rosenbloom MH, Alkalay A, Agarwal N, Baker SL, O'Neill JP, Janabi M, et al. Distinct clinical and metabolic deficits in PCA and AD are not related to amyloid distribution. Neurology 2011; 76: 1789–1796.

Ross SJ, Graham N, Stuart Green L, Prins M, Xuereb J, Patterson K, et al. Progressive biparietal atrophy: an atypical presentation of Alzheimer's disease. J Neurol Neurosurg Psychiatry 1996; 61: 388–95.

Salloway S, Sperling R, Gilman S, Fox NC, Blennow K, Raskind M, et al. A phase 2 multiple ascending dose trial of bapineuzumab in mild to moderate Alzheimer disease. Neurology 2009; 73: 2061–70.

Sambataro F, Murty VP, Callicott JH, Tan HY, Das S, Weinberger DR, et al. Age-related alterations in default mode network: impact on working memory performance. Neurobiol Aging 2010; 31: 839–52.

Seeley WW, Crawford RK, Zhou J, Miller BL, Greicius MD. Neurodegenerative diseases target large-scale human brain networks. Neuron 2009; 62: 42–52.

Sheline YI, Raichle ME, Snyder AZ, Morris JC, Head D, Wang S, et al. Amyloid plaques disrupt resting state default mode network connectivity in cognitively normal elderly. Biol Psychiatry 2010; 67: 584–7.

Shiino A, Watanabe T, Kitagawa T, Kotani E, Takahashi J, Morikawa S, et al. Different atrophic patterns in early- and late-onset Alzheimer's disease and evaluation of clinical utility of a method of regional z-score analysis using voxel-based morphometry. Dement Geriatr Cogn Disord 2008; 26: 175–86.

Shirer WR, Ryali S, Rykhlevskaia E, Menon V, Greicius MD. Decoding subject-driven cognitive states with whole-brain connectivity patterns. Cereb Cortex 2012; 22: 158–165.

Smith SM, Fox PT, Miller KL, Glahn DC, Fox PM, Mackay CE, et al. Correspondence of the brain's functional architecture during activation and rest. Proc Natl Acad Sci USA 2009; 106: 13040–5.

Snowden JS, Stopford CL, Julien CL, Thompson JC, Davidson Y, Gibbons L, et al. Cognitive phenotypes in Alzheimer's disease and genetic risk. Cortex 2007; 43: 835–45.

Sorg C, Riedl V, Muhlau M, Calhoun VD, Eichele T, Laer L, et al. Selective changes of resting-state networks in individuals at risk for Alzheimer's disease. Proc Natl Acad Sci USA 2007; 104: 18760–5.

Tang-Wai DF, Graff-Radford NR, Boeve BF, Dickson DW, Parisi JE, Crook R, et al. Clinical, genetic, and neuropathologic characteristics of posterior cortical atrophy. Neurology 2004; 63: 1168–74.

Tenovuo O, Kemppainen N, Aalto S, Nagren K, Rinne JO. Posterior cortical atrophy: a rare form of dementia with in vivo evidence of amyloid-beta accumulation. J Alzheimers Dis 2008; 15: 351–5.

van der Flier WM, Pijnenburg YA, Fox NC, Scheltens P. Early-onset versus late-onset Alzheimer's disease: the case of the missing APOE epsilon4 allele. Lancet Neurol 2011; 10: 280–8.

Walsh DM, Selkoe DJ. A beta oligomers—a decade of discovery. J Neurochem 2007; 101: 1172–84.

Wang K, Liang M, Wang L, Tian L, Zhang X, Li K, et al. Altered functional connectivity in early Alzheimer's disease: a resting-state fMRI study. Hum Brain Mapp 2007; 28: 967–78.

Whitwell JL, Jack CR Jr, Przybelski SA, Parisi JE, Senjem ML, Boeve BF, et al. Temporoparietal atrophy: a marker of AD pathology independent of clinical diagnosis. Neurobiol Aging 2011; 32: 1531–41.

Whitwell JL, Jack CR, Kantarci K, Weigand SD, Boeve BF, Knopman DS, et al. Imaging correlates of posterior cortical atrophy. Neurobiol Aging 2007; 28: 1051–61.

Zhou J, Gennatas ED, Kramer JH, Miller BL, Seeley WW. Predicting regional neurodegeneration from the healthy brain functional connectome. Neuron 2012; 73: 1216–27.